Formation of Thin Oxide Films by Metal-Organic Chemical Vapour Deposition

V.A.C. Haanappel, H.D. van Corbach, R. Hofman, R.W.J. Morssinkhof, T. Fransen* and P.J. Gellings

University of Twente, Department of Chemical Technology, P.O. Box 217, 7500 AE Enschede, The Netherlands

ABSTRACT

A summary is given of the metal-organic vapour deposition, performed during the last eight years at the University of Twente (The Netherlands), of thin alumina, silica, and titania films at atmospheric and at low pressure on stainless steels. Alumina films were produced from aluminium-tri-sec-butoxide (ATSB) and aluminium-tri-iso-propoxide (ATI), silica films from di-acetoxy-di-t-butoxy-silane (DADBS), and titania films from titanium-tetra-iso-propoxide (TTIP). These investigations can be separated into a number of projects: 1) mechanistic aspects of the decomposition chemistry of the precursors, 2) kinetics of the deposition processes, 3) chemical properties, and 4) mechanical properties of the thin oxide films.

INTRODUCTION

The production of thin oxide films by metal-organic chemical vapour deposition can be performed at relatively low temperatures. These films can be used for a variety of applications, such as in micro-electronics, as optical filters and as corrosion and wear resistant layers. Chemical vapour deposition (CVD) involves the activation of a gaseous reactant, also called precursor, which decomposes thermally (pyrolytically) or reacts with other gaseous species to a solid product. This can be carried out either homogeneously or heterogeneously. The homogeneous reaction generally results in the formation of powder, whereas the heterogeneous reaction results in the deposition of a coating on a substrate surface. For the formation of thin layers, two types of reactors are used. Most common is the activation by resistance heating, in a so-called "hot wall reactor" consisting of a reactor tube surrounded by a furnace. Less common is the "cold wall reactor" where only the substrate is heated. Advantages of the latter are a strongly reduced homogeneous gas phase reaction and no deposition on the reactor walls. The major advantage of the hot wall reactor is that there are no restrictions regarding the dimensions of the coated surfaces. Hence, many variations of the CVD technique have been developed in the last decades, such as conventional CVD, low pressure CVD, laser-assisted CVD, plasma-enhanced CVD and metal-organic CVD (MOCVD) /1-5/. Advantages of the CVD processes include the relatively low costs of the equipment, and the possibility of both batch and semicontinuous operation /3/.

MOCVD differs from other CVD techniques in the chemical nature of the precursor. In this process, gas-phase metal-organic molecules are decomposed to materials such as oxides, nitrides and metals. MOCVD involves low temperatures for the deposition of coatings which can be of particular importance because the properties of the substrate could deteriorate if too high temperatures are used. In the past ten years, much research has been performed on MOCVD /4-6/.

In this paper a summary is presented with respect to the deposition of thin alumina, silica and titania films

* To whom all correspondence should be addressed.

performed at the University of Twente during the last eight years (March 1987–March 1995). In addition to the decomposition mechanisms of several precursors (metal alkoxides, the kinetics of the deposition process and the chemical and mechanical properties of the deposited oxide films are also presented.

EXPERIMENTAL PROCEDURES

Specimen preparation

Depositions were performed on AISI 304 (18% Cr, 8% Ni, 0.08% C, 1% Si, 2% Mn, 71% Fe) and Incoloy 800H (20% Cr, 32% Ni, 0.08% C, 0.5% Si, 0.7% Mn, 0.4% Al, 47% Fe). The samples were cut from an electropolished sheet or were ground on SiC paper with a final size of 4000 grit, followed by a polishing treatment with alumina (3 μm) and subsequently ultrasonically cleaned for 30 minutes in RBS soap, hexane and ethanol. Finally, the samples were immersed in Struer's etching fluid (5% solution of 3 M nitric acid in ethanol) for 15 minutes, washed with pure ethanol and dried in air at room temperature.

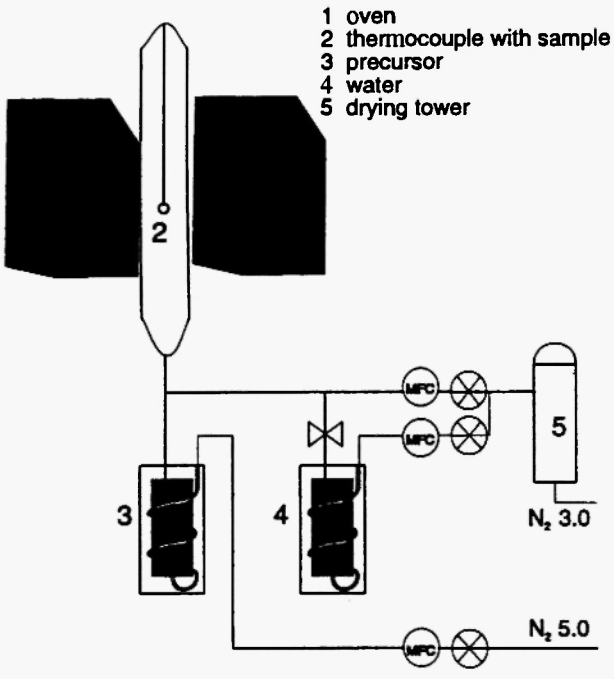

Fig. 1: Schematic view of the experimental MOCVD set up /6/.

Atmospheric-pressure Al_2O_3-deposition using ATSB

Alumina films were produced by decomposing aluminium-tri-sec-butoxide (ATSB, Janssen Chimica) under atmospheric circumstances. A schematic view of the experimental apparatus is given in Figure 1. A stream of pure nitrogen gas was passed through a coil in a silicone oil bath at 138°C where the nitrogen gas was saturated with the ATSB. The resulting gas was mixed with another nitrogen gas stream to achieve the required concentration of the precursor before entering the reaction tube. The sample was attached to a ceramic tube with a thermocouple inside for accurate measurement of the temperature. The standard conditions for the MOCVD-process were: silicone oil bath with ATSB: 138°C, carrier gas flow (N_2): 1300 ml/min (STP), diluent gas flow (N_2): 5200 ml/min (STP), substrate temperature: 330°C. A part of the diluting gas stream could be passed through a water saturator.

Low-pressure Al_2O_3-deposition using ATSB

The Al_2O_3 coatings were deposited by pyrolysis of ATSB (Janssen Chimica) in an LPCVD system, schematically depicted in Figure 2. It consisted of a horizontal quartz tube reactor (134 cm long, 10 cm in diameter) in a three-zone furnace (Tempress model Omega Junior). A stream of pure nitrogen gas (Praxair nitrogen 5.0) passed through the ATSB precursor in a silicone oil bath. This saturated gas was then diluted with pure nitrogen gas before entering the reactor. The gas line between the ATSB container and the reactor was heated to 150°C to prevent condensation of the precursor. All gas streams were controlled by electronic mass flow controllers (Brooks 5850TR). The deposition temperature was monitored by 3 thermocouples which extended into the reactor below the specimens. The temperature profile was maintained as constant as possible (± 0.5°C) over the length of the specimen load. The reactor pressure during deposition was monitored by capacitive pressure sensors (MKS Baratron type 122A) and kept at the desired value by adding an excess flow of nitrogen to the vacuum pump (Leybold D65BCS). The standard conditions for the LP-MOCVD process were: silicone oil bath with ATSB: 134°C, carrier gas (N_2): 7 ml/min (STP), diluent gas flow (N_2): 994 ml/min (STP), substrate temperature: 280°C, reactor pressure: 1.25 torr (0.17 kPa).

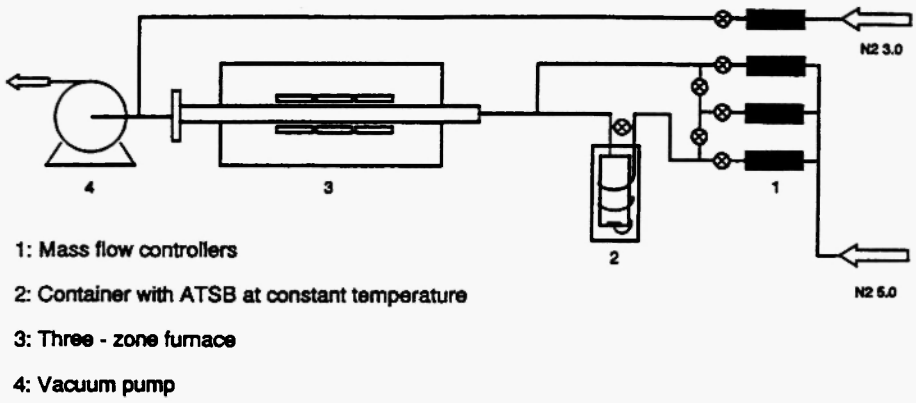

Fig. 2: Schematic view of the low pressure MOCVD set up /6/.

Atmospheric-pressure Al_2O_3-deposition using ATI

The deposition of alumina from aluminium-tri-iso-propoxide was performed in the same way as the atmospheric pressure deposition of alumina from ATSB. The standard conditions for the MOCVD-process were: silicone oil bath with ATI: 134°C, carrier gas flow (N_2): 3000 ml/min (STP), diluent gas flow (N_2): 7000 ml/min (STP), substrate temperature: 400°C.

Low-pressure Al_2O_3-deposition using ATI

The LP-MOCVD system used is described in the section "low-pressure alumina deposition using ATSB" and shown in Figure 2. The standard conditions for the MOCVD-process were: silicone oil bath with ATI: 110°C, carrier gas flow (N_2): 10 ml/min (STP), diluent gas flow (N_2): 990 ml/min (STP, substrate temperature: 350°C, reactor pressure: 3.5 torr (0.48 kPa).

Atmospheric-pressure SiO_2-deposition using DADBS

SiO_2-coatings were produced by the decomposition of di-acetoxy-di-t-butoxy-silane (DADBS). The standard conditions for the MOCVD-process were: silicone oil bath with DADBS: 80°C, carrier gas flow (N_2): 400 ml/min (STP), diluent gas flow (N_2): 400 ml/min (STP), substrate temperature: 560°C. A part of the diluting gas stream could be passed through a water saturator.

Atmospheric-pressure TiO_2-deposition using TTIP

TiO_2-coatings were produced by the decomposition of titanium-tetra-iso-propoxide. The standard conditions for the MOCVD-process were: silicone oil bath with TTIP: 70°C, carrier gas flow (N_2): 750 ml/min (STP), diluent gas flow (N_2): 2250 ml/min (STP), substrate temperature: 350°C.

Gas analysis

The residual gas analysis of the outlet gas streams was performed with a quadrupole mass spectrometer (SpectraMass-Dataquad), located at the exit of the reactor. The Dataquad provided monitoring of the current from the ion detector as a function of the mass-charge ratio (M/e). The mass spectrometer was connected to an Alcatel rotary pump, Model 2002B and a Balzers turbo molecular high-vacuum pump with electronic controller. Gas samples were drawn by the rotary pump into a stainless steel capillary. Samples were taken every minute until the gas composition reached a steady-state value. The intensity of a number of characteristic peaks was measured.

Corrosion experiments

Corrosion experiments were performed in order to investigate the protective capacity of the films against aggressive gas components, such as oxygen and sulphur at high temperatures, and were carried out in a closed

system for 24 h. The system was first flushed with argon for 20 h with a flow rate of 16 $l.h^{-1}$. The argon was saturated with water at 15°C. After this, a mixture of 5% H_2S in H_2 with a flow rate of 4 $l.h^{-1}$ was introduced in the argon flow. After 2 h, in order to stabilize the flow, the furnace was heated to the test temperature (450°C). The whole system was flushed for another 2 h and then closed. It was previously found /6/, that no relevant difference in corrosion rate and corrosion products was obtained between a closed system and a system with a continuous flow, if the reactive gas consumption did not exceed 20%.

The morphology and the composition of the corroded specimens were investigated by means of optical and scanning electron microscopy (JEOL M 35 CF), the latter equipped with an EDX analysis system (Kevex Delta - class III).

Chemical properties

To characterize the chemical composition and the depth profile, the oxide films were analyzed using a Perkin-Elmer PHI 600 scanning Auger multiprobe. Alternative sputtering and Auger analysis were used during in-depth analysis. The functional groups, including hydrogen-containing bonds within the films, were measured by Fourier transform infrared spectroscopy (FTIR), using a Nicolet 20 SX FTIR apparatus. Due to the non-transparency of the specimens, the spectrometer was equipped with a diffuse-reflection cell /5/. The micro-structure of the films was investigated by X-ray diffraction (XRD), using a Philips PW 1710 X-ray Diffractometer with monochromatic CuKα-radiation and a high resolution transmission electron microscope (TEM), model JEOL 200 CX. The refractive index of the deposited films was measured with a Plasmos ellipsometer (type SD 2002) at a wavelength of 6328 Å using a He-Ne laser source. The angle of incidence was 70°.

Mechanical properties by hardness and scanning scratch test measurements

Indentation experiments were performed with the hardness tester DUH-200, developed by Shimadzu. The major specifications of the Shimadzu Dynamic Ultra Micro Hardness Tester DUH-200 are: loading method: electromagnetic coil, load range: 0.01 gf to 200 gf, indentation depth measuring method: differential transformer, indentation depth measuring range: 0 to 12 μm, indentation depth readability: 0.001 μm, diagonal length measuring unit: optical encoder, and diagonal length display resolution: 0.1 μm. Three types of testing were possible /6/: 1) the load/load-hold test mode used to obtain the dynamic hardness of a specimen from the total indentation depth at the end of the after time, 2) the cyclic load-unload test mode, where the loading and unloading up to a certain level is repeated to observe changes in plastic deformation and elastic deformation, and 3) the load with correction-load hold mode, which is often used to observe changes in deformation in soft materials.

The low load indentation experiments were performed with a Vickers indenter (top angle: 136°). The maximum load was 2 gf. The loading speed was $2.9\ 10^{2}$ $gf.s^{-1}$ with a hold time of 5 s. The indentation fracture tests were performed with a load of 150 gf, a loading speed of 1.44 $gf.s^{-1}$ and a hold time of 5 s.

Scanning scratch adhesion measurements were performed with a SSTT-101 scanning scratch tester developed by Shimadzu. The adhesion of thin films was evaluated by the load (critical load), at which the film started to peel by scratching with a hard stylus. A detailed description of the equipment is given elsewhere /6/. The specific parameters of the SST-101 for the thin oxide films were: stylus tip radius: 25 μm, amplitude: 50 μm, down speed: 1 μm/s and stage drive speed along the Y axis: 20 μm/s.

RESULTS AND DISCUSSION

Mechanistic and Kinetic Aspects

Mechanistic aspects of oxide deposition by MOCVD

The decomposition mechanism of ATI during the deposition process of thin alumina films was studied by Morssinkhof /5/ using a differential scanning calorimeter (Stanton Redcroft System III), a Setaram TG-85, a quadrupole mass spectrometer (SpectraMass-Dataquad), and a Nicolet 20-SXC FTIR spectrophotometer. Thermogravimetry showed that the decomposition of ATI follows a two-step mechanism. The first

started around 200°C and the second at about 280°C. The decomposition products were analysed by mass spectrometry (MS) and FTIR. During the deposition process only two compounds were detected in a reasonable amount, propene and isopropanol, together with traces of water. Figure 3 shows the normalized intensity of isopropanol and propene as a result of a temperature-programmed decomposition of ATI. From the amount and distribution of the reaction products a model for the decomposition mechanism is proposed. This model is based on a β-hydride elimination mechanism by the occurrence of a rather stable monomeric six-ring with intramolecular bond formation between the Al-O group and the hydrogen attached to the β-carbon. During the first step propene and isopropanol will be formed, followed by a second step involving the elimination of the last isopropoxide group, resulting in a boehmite molecule and propene. In addition to these gas phase reactions, it was proposed that the boehmite adsorbs on the substrate surface followed by a reaction forming alumina and water. The adsorption was described by a Langmuir adsorption mechanism. Morssinkhoff /5/ only paid attention to the formation of alumina by the β-hydride elimination mechanism. Nothing was reported about the existence and the contribution of a free-radical – or an α-hydride elimination mechanism – to the overall mechanism.

Research on the decomposition of ATSB using a quadrupole mass spectrometer (SpectraMass-Dataquad) was performed by Haanappel /6,7/. It was found that the main by-products from the pyrolytic decomposition of ATSB were 2-butanol, 2-butanone, 1- or 2-butene, and n-butane. No changes in the type and concentration of the products were observed upon addition of small amounts of water. Only the heterogeneous reaction was altered due to the presence of small amounts of water. This is in contrast with the proposal of Morssinkhof /5/ to describe the decomposition mechanism of ATI. In that case it was suggested that the presence of some water may accelerate or catalyse the formation of isopropanol. Attention has been paid to three different decomposition mechanisms: 1) a free radical, 2) a β-hydride elimination, and 3) an α-hydride elimination mechanism, all based on data from Desu /8/. Based on the products formed during thermal cracking of the

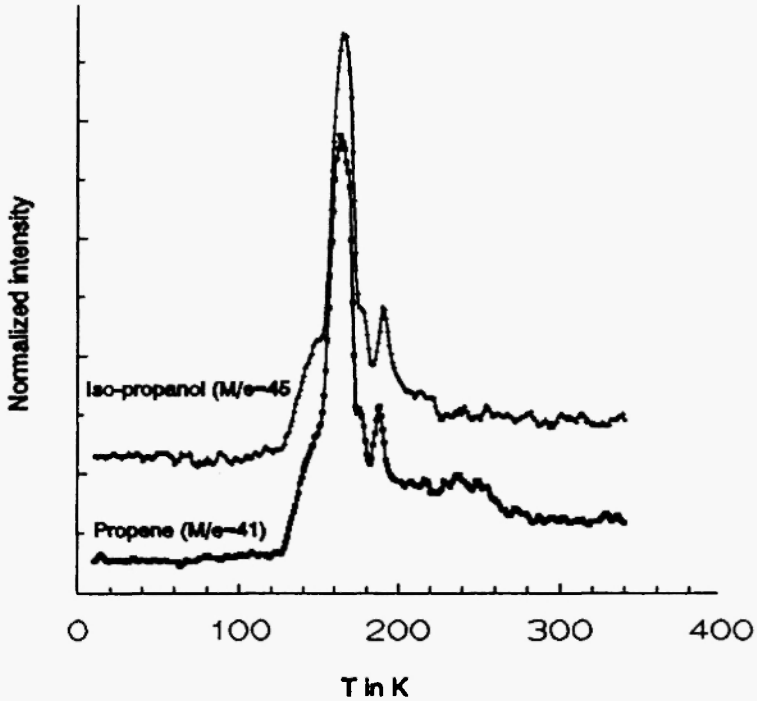

Fig. 3: Temperature-programmed decomposition followed with mass spectrometer, at m/e = 41 (PP) and m/e = 45 (IPA) /5/.

ATSB, it was found that the β-hydride elimination dominates the decomposition mechanism. The other mechanisms, the free radical – and the α-hydride elimination – probably play only a minor role. This was explained by the large volume of the alkyl group of the metal-organic compound ATSB. The alkyl group of the compound ATI is smaller, indicative of the possibility to decompose partly by an α-hydride elimination mechanism. Therefore, it is assumed that, in addition to ATSB, ATI may also decompose to a minor extent by a free radical and/or an α-hydride elimination mechanism. In Figure 4 details of the β-hydride elimination mechanism of the gas-phase decomposition of ATSB are shown.

In addition to the decomposition of alumina-forming metal alkoxides, Hofman /4,9/ studied the decomposition of DADBS in a nitrogen atmosphere at atmospheric pressure. It was found by quadrupole mass spectrometry that the recorded peak intensities of the reaction products acetic acid anhydride were a function of the temperature, as shown in Figure 5. Products like acetic acid and 2-methyl-propanol were never observed. From the product quantity and distribution Hofman /4,9/ concluded that the pyrolysis of DADBS took place in three steps: 1) at temperatures higher than 200°C acetic acid anhydride is formed, 2) at temperatures higher than 400°C 2-methyl-propene is formed, and 3) the remaining silicone acid is converted to silica by a poly-condensation reaction. The decomposition mechanism is based on the formation of a stable six-ring, followed by a β-hydride elimination mechanism. According to the model of these reactions, Hofman /4/ developed reaction kinetics describing homogeneous gas-phase and heterogeneous surface reactions following the Langmuir adsorption theory.

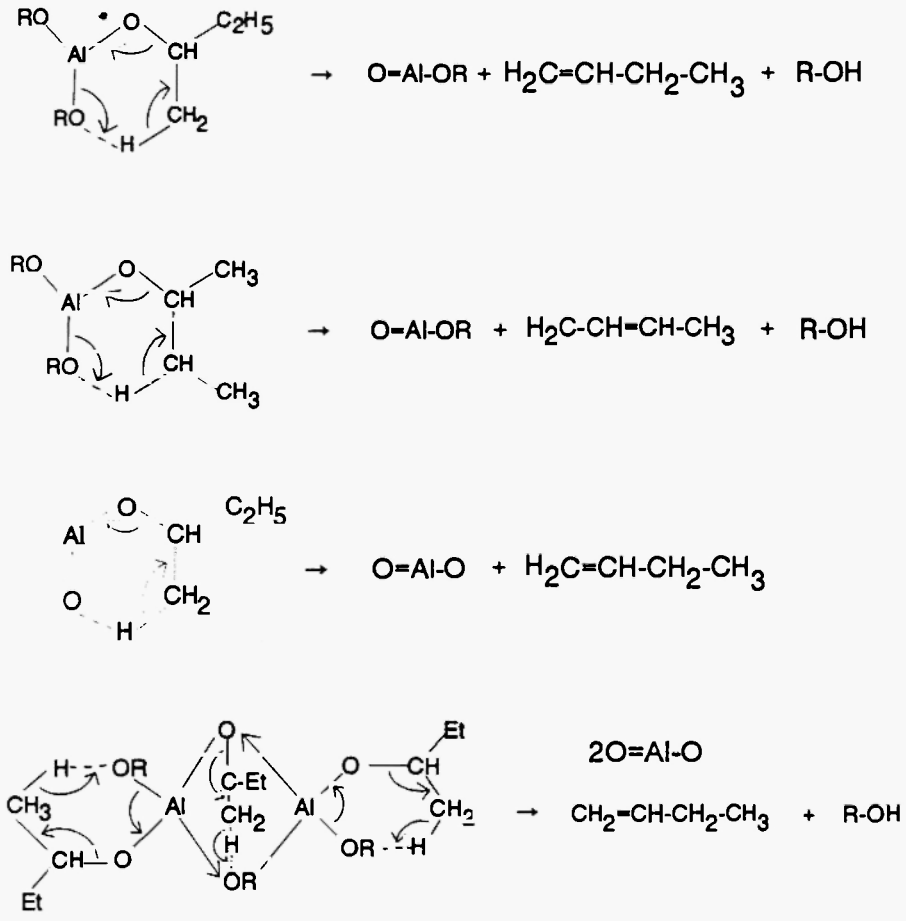

Fig. 4: Details of the β-hydride elimination mechanism of the gas phase decomposition of ATSB (R is CH_3 - CH - CH_2 - CH_3) /6,7/.

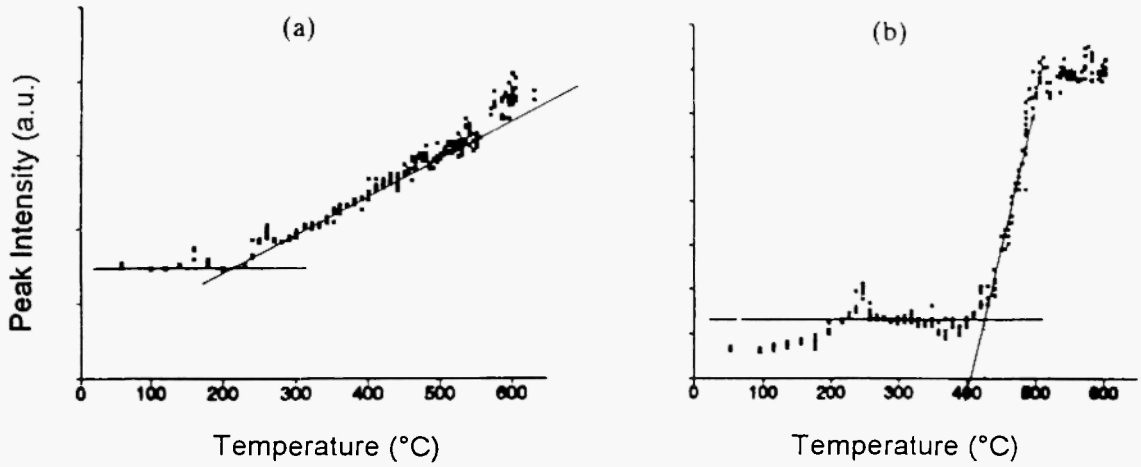

Fig. 5: Peak intensities (arbitrary units vs temperature) of acetic acid anhydride (a) and 2-methyl propene (b) as a function of the temperature /5,9/.

From these results it may be concluded that the decomposition mechanism of metal alkoxides during the deposition process can be described by three different mechanisms: an α-hydride elimination, a β-hydride elimination, and a free-radical mechanism. Depending on the steric hindrance of the alkyl group, the dissociation energy between different bonds, and the reaction circumstances, one of these may dominate the decomposition mechanism of the metal-organic compound during the MOCVD /4-6/.

Kinetic aspects of MOCVD

To determine the experimental activation energy (E_a) of the atmospheric pressure metal-organic chemical vapour deposition of thin alumina films using ATI (aluminium-tri-isopropoxide) as a precursor, the reactor temperature was varied over a range between 200 and 500°C /5/. The E_a for the formation of alumina was about 30 kJ/mole at lower temperatures which decreased to lower values at higher temperatures, especially above 420°C. This was due to the change from a reaction-rate-limited to a diffusion-rate-limited growth. The diffusion-rate-limited growth above 420°C was confirmed by studying the growth rate as a function of the total flow rate at 420°C /6/. The growth rate was found to be proportional to the flow rate by a square root relation. This is explained by a change of the deposition regime from a rate control by surface reaction (at low temperatures) to a rate control by mass transport in the diffusion boundary layer (at high temperatures). With increasing temperature, the surface reaction rate increases much faster than the diffusion rate through the boundary layer. Ultimately, the diffusion rate will dominate the overall deposition rate. The reaction order was determined at 400°C by changing the precursor concentration and was calculated to be a first order. No experiments were performed at lower temperatures. At 400°C the effect of the diffusion rate through the stagnant boundary layer may affect the growth rate, indicative of a possible change of the reaction order with decreasing temperature. From these results standard conditions were chosen, as reported in the section "Experimental". In addition to the atmospheric pressure MOCVD, Morssinkhof /5/ also performed low-pressure MOCVD. Here also, an E_a of 30 kJ/mole was found. Changing the precursor concentration revealed a second-order reaction. The surface reaction rate (second order in ATI at relatively high concentrations) is given by:

$$\text{reaction rate} = k_{r,ATI}\,[ATI]^2_{surf}$$

where $k_{r,ATI}$ is the rate constant of the surface reaction of ATI ($m^4.moles^{-1}.s^{-1}$) and $[ATI]_{surf}$ is the concentration of ATI ($moles.m^{-3}$) near the surface of the specimen. Using the stagnant film model, the mass flux of the reactive component ATI through the diffusion boundary layer is given by:

$$J_{ATI} = k_g\,([ATI]_{bulk} - [ATI]_{surf})$$

where J_{ATI} is the flux of ATI through the boundary layer (moles.m^{-2}.s^{-1}) $[ATI]_{bulk}$ is the concentration of ATI (moles.m^{-3}) in the bulk, and k_g is the mass transfer coefficient in the gas phase (m.s^{-1}). In the steady state the reaction rate = J_{ATI}, resulting in a more complex equation for the reaction rate as a function of $[ATI]_{bulk}$, whereas the use of ATSB (first order in ATSB) has led to a more simple equation. This second-order reaction was explained by a Langmuir type adsorption of AlO(OH) and iso-propanol. This model was based on a relation between the growth rate, the partial pressure of the reactive compounds and their energies of activation.

Atmospheric deposition of alumina films using ATSB was performed by Haanappel /6/. The experimental activation energy was 83 ± 5 kJ/mole, calculated from the reaction-rate-limited film growth. The effect of the deposition temperature on the film growth is shown in Figure 6 /6/. Between 330–420°C, the deposition rate of alumina is about first order (1.0 ± 0.2) with respect to the initial concentration of ATSB. Furthermore, at temperatures starting from 400°C the deposition rate was also a function of the gas flow, indicative of diffusion-rate-limited film growth. This corresponds well with the simple mathematical model /6,10/ of the MOCVD-process, following:

$$J = [ATSB] / (1/k_r + 1/k_g)$$

where

J	=	deposition rate
[ATSB]	=	concentration of ATSB
k_f	=	rate constant of the surface reaction
$k_g = (D.\delta)$	=	mass transfer coefficient in the gas phase
D	=	diffusion coefficient
δ	=	thickness of diffusion boundary layer

Two extreme situations were observed: for $k_r/k_g \gg 1$ the deposition rate is determined by diffusion-limited growth, and for $k_r/k_g \ll 1$, the deposition rate is limited by the reaction. This equation implies that under reaction-rate-limited circumstances, the deposition rate is at a given concentration of ATSB, only a function of k_r, whereas it is only a function of k_g if the reaction is completely diffusion-controlled. This means that, if limitation by diffusion occurs, the deposition rate is

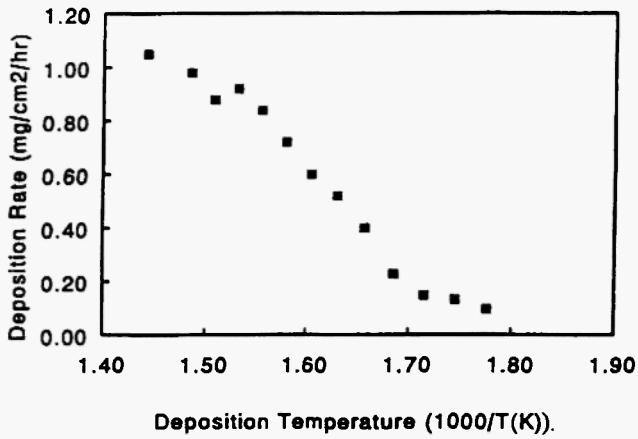

Fig. 6: Deposition rate of alumina as a function of the deposition temperature (K) /6/.

also a function of the total flow rate. At higher temperatures the deposition rate will increase proportionally to the flow rate. The mass transfer coefficient, k_g, in the gas phase can also be written as the ratio between the diffusion rate constant D and the thickness, δ, of the stagnant diffusion boundary layer, D/δ, with

$$\delta = [(\mu.x) / (\rho.v)]^{1/2}$$

where μ is the dynamic viscosity (kg.m^{-1}.s^{-1}), x is the position on the specimen surface (m), ρ is the density of the gas (kg.m^{-3}), and v is the gas velocity (m.s^{-1}). In order to prevent non-uniform film thicknesses, low-pressure MOCVD was performed. The major difference between the atmospheric and the low-pressure MOCVD is the enhancement of the mass flux of gaseous reactants and products through the stagnant boundary layer between the gas bulk phase and the specimen surface in the latter case. The most important variables were the ATSB partial pressure and the total gas flow through the reactor. From Morssinkhof's /5/ results a precursor partial pressure between 5.5 x 10^{-4} and 33.5 x 10^{-4} kPa and a deposition temperature between 200 and 380°C (LP-MOCVD) was most promising. At higher ATSB partial pressures, the coatings were covered with a small amount of powder. This indicated that the products from a homogeneous reaction of ATSB to Al_2O_3 in the gas phase were partly deposited on the specimen surface. At lower ATSB partial pressures, it

was more difficult to obtain a homogeneous and uniform coating: the bulk concentration of ATSB in the gas phase was probably too low. The total gas flow was 1 l/min (STP), corresponding to about 13 cm/min (STP). From the Arrhenius plot, the experimental activation energy was calculated to be 65 ± 2 kJ/mole. The order of the reaction with respect to ATSB was determined at a deposition temperature of 270°C and a reactor pressure of 0.17 kPa. It was found that the reaction was first order, decreasing with increasing precursor concentration to zero and then increasing again. This may be explained by a Langmuir type adsorption as already discussed by Morssinkhof /5/. Another explanation is given by Corbach /11/. When the ATSB partial pressure is increased to a value where the slope of the plot is zero, there is probably a diffusion limitation of reactive molecules, while with a further rise in ATSB partial pressure, Al_2O_3 powder from the homogeneous reaction will deposit on the specimen causing the rise in experimental growth rate. From these results and the sulphidation experiments, discussed later, optimum conditions were obtained as reported in the section "Experiments".

Determination of the kinetics of SiO_2 deposition by atmospheric-pressure MOCVD was performed by Hofman /4,12/. From the Arrhenius plot (low-concentration region) the experimental activation energy was determined to be 150 kJ/mole. The reaction order, studied at 560°C, was found to increase from 1 in the low-concentration region to 1.6 in the high-concentratio9n region. Hofman /4/ suggested that this could be explained by two parallel reactions, a first and a second order reaction, both rate-influencing, according to:

$$\text{reaction rate} = k_1 C_{DADBS} + k_2 C^2_{DADBS}$$

where k_1 and k_2 are reaction rate constants, and C_{DADBS} the concentration of DADBS, respectively. This model is coupled to the decomposition chemistry of DADBS. Furthermore, the influence of water on the deposition rate was also studied. The deposition reaction of silica was inhibited by the presence of small amounts of water. The order of the inhibition reaction was found to be 0.5.

From the growth rate of TiO_2 as a function of the deposition temperature, it was shown that at 315°C the reaction-rate-limited growth changes to the diffusion-rate-limited growth. The experimental activation energy, calculated from the slope of the reaction-rate-limited growth section, was 79.0 ± 0.1 kJ/mol. This is of the same order of magnitude as for Al_2O_3. The growth rate as a function of the precursor partial pressure was determined at two deposition temperatures. At 300°C the slope of the plot (ln(growth rate) versus ln(concentration)) was calculated to be 0.47 ± 0.05, while at 350°C the slope was 0.69 ± 0.05. The layer thickness versus deposition time revealed a linear relationship over the test time range (0 - 120 min). After a deposition time of 120 minutes the layer thickness was 5 μm.

Chemical Properties of Thin Oxide Films

Corrosion experiments

Corrosion experiments to determine the protective capacity of several oxide films were performed at elevated temperatures in a sulphidizing atmosphere. Sulphidation experiments were carried out for all oxide films, 1) alumina from ATI, deposited at atmospheric and low pressure /5/, 2) alumina from ATSB (with and without small amounts of water) at atmospheric and low pressure /6/, 3) silica from DADBS (with and without small amounts of water) at atmospheric pressure /4/, and 4) titania from titanium-tetra-iso-propoxide (TTIP) at atmospheric pressure /13/.

Morssinkhof /5/ used Incoloy 800H as a substrate material for the deposition of thin alumina films. From the corrosion experiments it was found that the corrosion resistance increased with increasing deposition temperature. The sulphidation resistance was further increased by treating the coated samples in air at 850°C, as shown in Figure 7. Sulphidation experiments were performed at 550°C in 1% H_2S, 1% H_2O, 19% H_2, and bal. Ar. This improvement was explained by the formation of chromia in the cracks and pores. An increased protectivity of the alumina films against sulphidation with increasing deposition temperature was also found by Haanappel /6/. Figure 8 shows the relative weight gain of alumina films deposited at atmospheric pressure on AISI-304 as a function of the deposition temperature. In this case the sulphidation

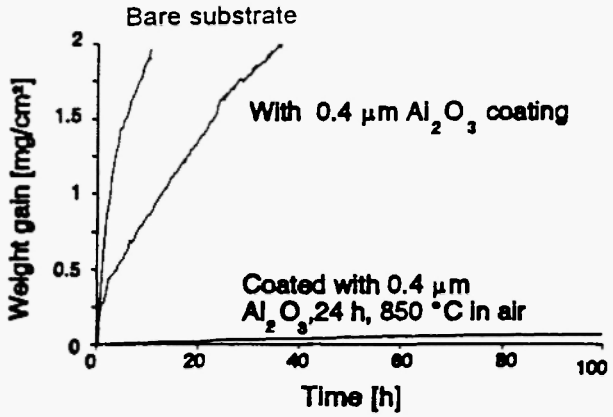

Fig. 7: The effect of heat treatment on the sulphidation resistivity of alumina-coated Incoloy 800H, deposited at 300°C. Sulphidation experiments were performed at 550°C in 1% H_2S, 1% H_2O, 19% H_2, and bal. Ar /5/.

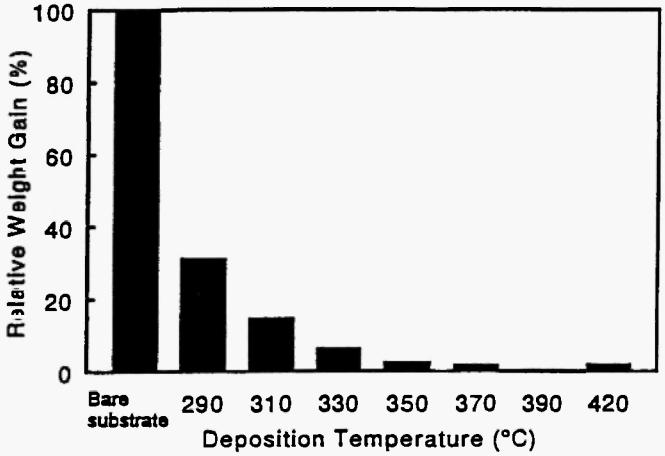

Fig. 8: Bar diagram of the relative weight gain (%) of alumina-coated AISI 304 (after 24 hr sulphidation at 450°C) as a function of the deposition temperature. The sulphidation experiments were performed during 24 hr at 450°C in 1% H_2S, 1% H_2O, 19% H_2, and bal. Ar /6/.

experiments were performed during 24 hr at 450°C in 1% H_2S, 1% H_2O, 19% H_2, and bal. Ar. Thermal annealing or addition of small amounts of water at the gas stream did not improve the protectivity of the films, deposited at atmospheric pressure from ATSB. Cracks and pores were still present. On the other hand, reducing the reactor pressure significantly improved the corrosion resistance. Especially at a deposition temperature of 280°C, no weight gain was observed any more (reactor pressure: 0.17 kPa, ATSB partial pressure: $7.5.10^{-4}$ kPa).

The degradation mechanism of silica films on AISI 304 /4/ during the sulphidation experiments corresponds well with that of alumina films /5,6/. Also here, the underlying substrate was exposed to the aggressive environment in the presence of cracks in which FeS is formed. Hofinan /4/ also paid attention to the thermodynamic and kinetic aspects of the formation of sulphides inside the existing cracks. In order to improve the resistance of silica coatings against sulphidation, small amounts of water were added to the gas flow. It was found that coatings prepared with a water partial pressure > 36 kPa were crack-free. This means that an increased water concentration can lead to a decrease in crack density and an improved corrosion resistance.

The optimum deposition temperature of titania films on AISI 304 regarding the corrosion protectivity (after 70 h at 450°C) was obtained by factorial design. Furthermore, coatings with a thickness of 1 µm were deposited at several temperatures, ranging from 290 to 410°C. The weight gain was measured after sulphidation at 500°C for 70 h. The experiments revealed that the weight gain decreased with increasing temperature up to 390°C. At this temperature, the relative weight gain decreased from 39% to 8% compared to an uncoated sample. At 410°C the relative weight gain was 20%. At a sulphidation temperature of 450°C the weight gain decreased with increasing film thickness, with no weight gain when using 5 µm TiO_2. No pores or cracks occurred on the surface.

From the results it is clear that the main cause for degradation of thin oxide films is the presence of cracks and pores. The existence of the cracks is generally related to the internal stress in the thin oxide films. Oxide films applied by MOCVD suffer in general from thermal and intrinsic stresses, according to:

$$\sigma_{internal} = \sigma_{intrinsic} + \sigma_{thermal}$$

These internal stresses may be generated by different

sources: during film formation and/or by thermal mismatch. The thermally induced part of the stress in alumina on steel can be calculated from the difference between the thermal expansion coefficients of the film and the metal, the difference between the deposition and the actual temperature, and Young's modulus of the film. The intrinsically induced part is caused by the growth mechanism of the alumina film.

The origin of the intrinsic stresses in the silica and alumina films is yet unclear. Morssinkhof /5/ reported that the large intrinsic stress may be explained by the presence of hydroxide groups in the oxide scale. However, the relationship between the incorporation of elements or groups of atoms and the critical coating thickness is not yet clearly understood. Hofman /4/ summarized and briefly discussed several possible mechanisms responsible for stress generation in silica films. The thermal stress can be reduced by minimizing the difference in thermal expansion coefficients. Since these are fixed, the thermal mismatch can only be reduced by one or more intermediate layers between the metal and the coating /4/. Preoxidizing of Incoloy 800H before applying a thin silica film did not result in a significant improvement of the sulphidation resistance. On the other hand, silica films prepared by using small amounts of water resulted in a significant stress reduction. This was based on elimination of cracks and an improved corrosion resistance. This stress relaxation in the silica films was explained by a decrease in the activation energy of viscous flow. The mechanism of the reduction in viscosity is assumed to be based on the increased OH-concentration in the silica film, where the hydroxide groups can participate in bond breaking and bond formation following a reversible reaction:

$$Si - OH + HO - SI \Rightarrow Si - O - Si + H_2O$$

The stress reduction was also determined by a shift of the Si-O-Si stretching band to lower and the Si-O-Si bending band to higher frequency.

This mechanism was also assumed to reduce the stresses in the alumina films using ATSB, following:

$$O = Al - OH + HO - Al = O \Rightarrow O = Al - O - Al = O + H_2O$$

Probably the activation energy for this reaction is much higher than in the case of silica. The porous structure of the alumina films, which was more pronounced for low than for high deposition temperatures, can be explained by the low conversion of the metal alkoxides or incorporation of AlO(OH) or H_2O into the film. For example, Yu /14/ reported that at low conversion of the metal alkoxides, the corresponding alcohol was identified in amounts of up to 1 mole per mole of the substance being decomposed. In a later stage the alcohol decomposes on the surface of the specimen.

Summarizing, it is seen that in the case of alumina films deposited on metallic substrates, only a heat treatment in air after deposition at high temperatures may lead to an improved sulphidation protection /5/, due to the formation of chromia inside the pores and cracks. Thermal annealing in nitrogen or the addition of small amounts of water did not improve the corrosion protectivity /6/. On the other hand, low-pressure MOCVD resulted in an improvement of the corrosion protection. No more cracks were found in the alumina film. In the case of silica films /4/, small additions of water to the gas flow have led to a significant improvement of the sulphidation protectivity; no more cracks or pores were found.

Chemical composition

The chemical composition of alumina films deposited by using ATI was investigated by AES and FTIR /5/. From the AES profiles it was clear that only O and Al were found as the elements in the alumina layer. After oxidation in air at 850°C, the sharp interface between the substrate, in this case Incoloy 800H, and the alumina film, had disappeared. This was explained by the complete miscibility of chromia and alumina. In the FTIR-experiments on coatings made at low deposition temperatures two peaks were observed, indicating the presence of OH (absorbance between 3000 and 3500 cm^{-1}) and Al-O groups (around 950 cm^{-1}). At higher deposition temperatures the OH-peak disappeared, whereas the peak of the Al-O bond increased in intensity and shifted towards higher wavenumbers; from 920 to 950 cm^{-1} at deposition temperatures from 250 t0 450°C, respectively. This shift was related to the intrinsic stress in the alumina film. Figure 9 shows the FTIR spectra of alumina-coated Incoloy 800H at various deposition temperatures

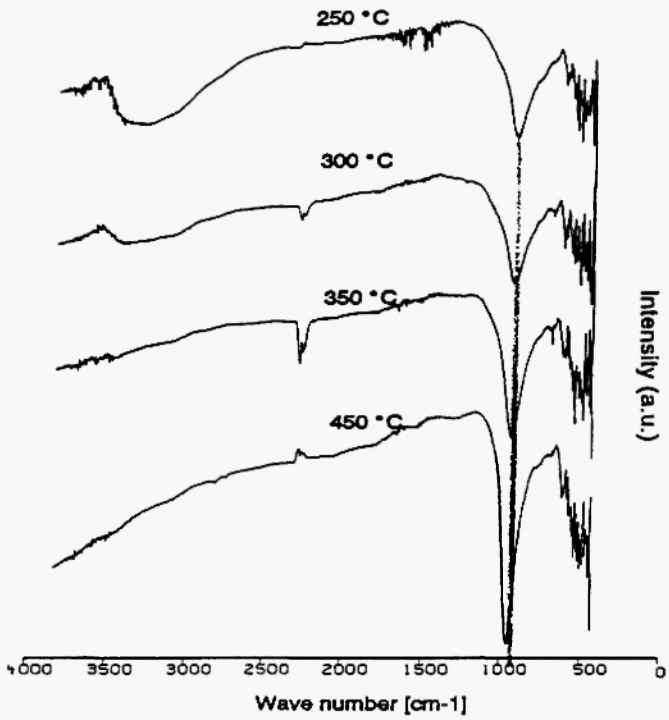

Fig. 9: FTIR spectra of alumina-coated Incoloy 800H, at various deposition temperatures /5/.

/5/. XRD analyses revealed that the alumina films had an amorphous structure. Heating to 800 and 1200°C resulted in a crystalline γ-alumina and α-alumina structure, respectively. TEM-analyses showed nano-crystalline phases of γ-alumina /5/.

Comparable results were obtained with AES and FTIR for the characterization of alumina films deposited with low- and atmospheric-pressure MOCVD using ATSB /6/. Here also, at high deposition temperatures the absorbance band for the OH-groups was reduced, and the Al-O band increased in intensity and shifted towards higher wavenumbers. After thermal annealing in nitrogen the OH-peak disappeared, whereas the Al-O peak shifted towards higher wavenumbers. The disappearance of the OH-band can be explained by the transition of boehmite to γ-alumina, following:

$$2\ AlO(OH) - Al_2O_3.(1-x)H_2O + xH_2O$$

The increased intensity of the Al-O IR absorption band and the change from a smooth, broad peak into a sharper one can be related to the decrease of the number of OH-groups /5/ and the transformation of an "amorphous" to a more crystalline material /6,15/. With AES, the composition and the depth profile of the deposited alumina films were analysed. No other elements were found than Al and O. Figure 10 shows the AES depth profile of the alumina film on AISI-304, deposited at atmospheric pressure and 400°C /6/. Only on the surface some carbon was detected, but after one sputtering cycle no carbon was detected any more above the background level of the equipment. Thermal annealing resulted in a less sharp interface, in agreement with the results of Morssinkhof /5/. The microstructure of the alumina films was investigated by XRD. From X-ray diffraction patterns of alumina films (atm. press.) deposited at various temperatures (290–420°C), no crystalline phases could be determined, indicating that the film has an amorphous structure /6/. Transmission electron micrographs of the alumina films deposited at 330°C show electron diffraction ring patterns, revealing an extremely fine grain size of the alumina film, between 8 and 20 mn. Similar results were obtained from alumina films deposited at low pressure or at atmospheric pressure with small water concentrations in the gas phase /6/.

To determine the chemical composition of silica films, FTIR and XPS were used /4/. It was found that with increasing water concentration in the vapour phase, the water peak between 3000 and 3500 cm^{-1} becomes less significant and the silanol peak at 3670 cm^{-1} becomes more important. This was explained /4,16/ by a larger OH : H_2O ratio, due to the reaction between the water molecules and the silica:

$$Si–O–Si + H_2O \Rightarrow Si–OH+HO–Si$$

From these observations it is clear that no other elements, except Si, O and H, were present in the silica film. XRD-analyses showed an amorphous structure of the silica films, deposited at 560°C. With TEM, small grains of silica with sizes between 10 and 18 nm were found. Electron diffraction patterns indicative of nano-crystalline phases were found here also /6/. No significant changes in the grain sizes were found if water was added to the gas stream. From these results it is clear that the oxide films, silica and alumina, did not differ very much as regards the grain size.

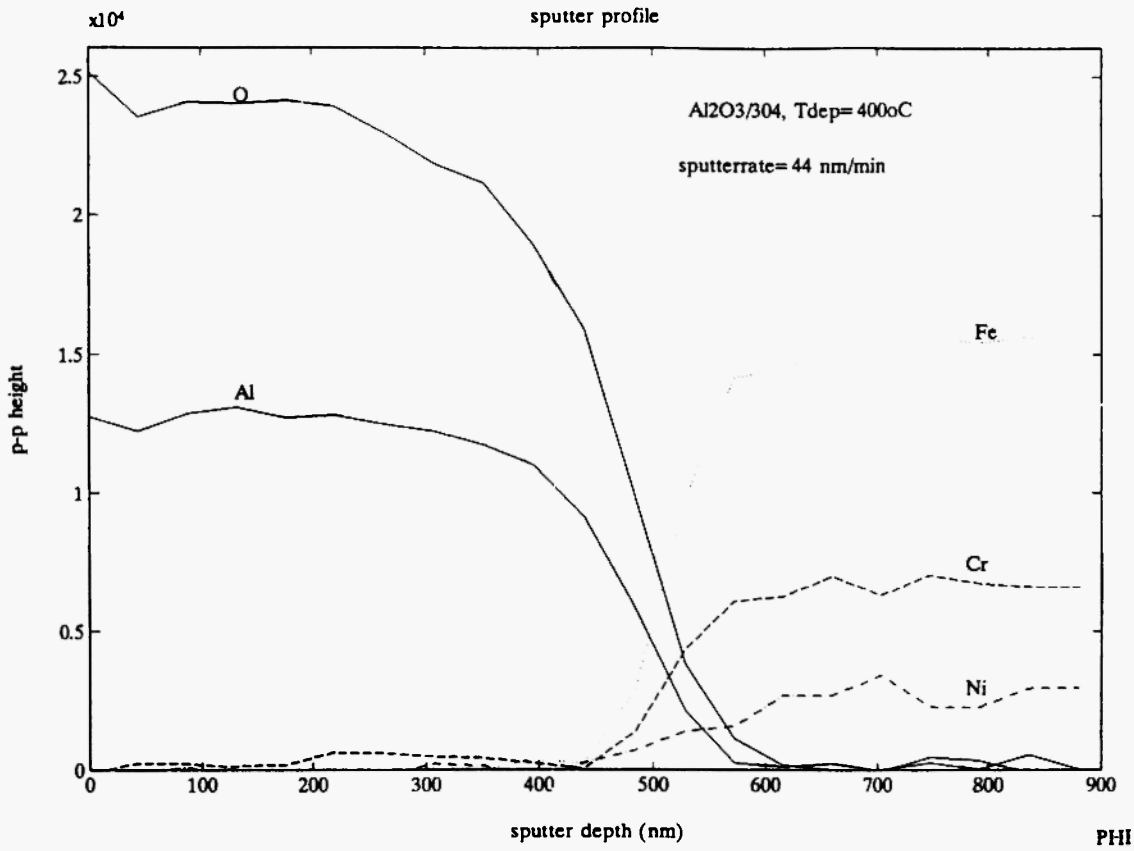

Fig. 10: AES depth profile analysis of the alumina film on AISI 304, deposited at 400°C /6/.

The chemical composition of titania films was studied by AES. It was found that only O and Ti were found as the elements in the titania layer. No carbon was detected, indicative of a complete conversion of the precursor to titania.

Refractive index

Only the refractive indices of the alumina films from ATBS deposited at atmospheric and low pressures were measured. The experimental index of refraction was found to vary in the range 1.53 – 1.60, increasing with the deposition temperature of the alumina film (atm. press.) in nitrogen, as shown in Figure 11 /6/. These values correspond with the value of amorphous alumina. The standard value for γ-alumina is about 1.7. Kang *et al.* /15/ suggested that the low value of the refractive index is also related to a low film density and hydrogen incorporation. For the thermal annealed specimens no refractive index could be measured, due to the change in interfacial composition profile change.

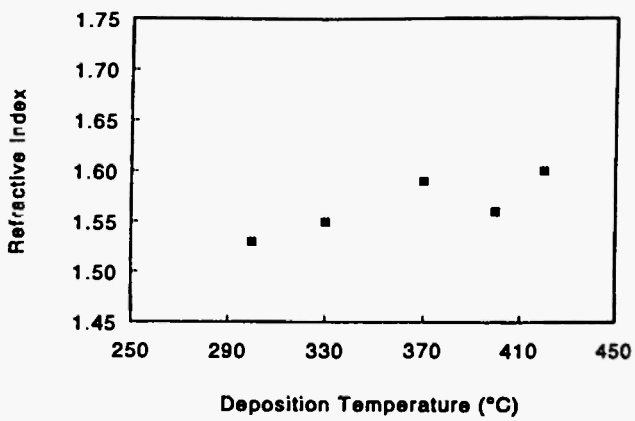

Fig. 11: Peak position of the Al-O bond, obtained from the FTIR absorbance spectra of alumina films, deposited at different temperatures /6/.

The effect of the underlying diffusion zone on the total value of index of refraction was not known. The refractive index of the alumina films, deposited at low pressure, varied between 1.62 and 1.70 depending on the deposition temperature.

Mechanical Properties of Thin Oxide Films

In addition to the review of several methods to measure the stress in thin films, such as X-ray diffraction and bending beam methods given by Morssinkhof /5/, an indirect method for stress determination has also been discussed. This method is based on the measurement of a corresponding stress in the substrate, just under the film, using the $\sin^2(\psi)$-method. It was found from the position and width of the diffraction peak that the stress increases with layer thickness and decreases with increasing deposition temperature. The internal stress resulted in an upper limit of the film thickness. Passing the critical thickness of the alumina film, cracking and delamination occurred.

To obtain more information about the mechanical properties of thin films, Hofman /4/ and Haanappel /6/ performed micro-hardness and scanning scratch tests. Hofman /4/ used indentation tests to quantify the hardness of the film. The major problem associated with the indentation tests of thin films is the indentation depth: the underlying substrate can affect the measurements. Only thick films or very small indentations give true hardness values. When the ratio indentation depth : film thickness exceeds a critical value, approximately between 0.07 and 0.2, the hardness is no longer a characteristic of the coating alone, since it is also influenced by the substrate material. Hofman /4/ used the Johnson–Hogmark relation /17/ to calculate the film hardness as a function of the water concentration during the MOCVD of silica films. From the loading-unloading curves the elastic modulus was also calculated. Figure 12 shows the loading-unloading curve for amorphous silica on Incoloy 800H /4/. It was found that addition of water during the deposition process did not change the hardness and elastic modulus of the silica film. Haanappel /6/ used the indentation instrument as an analytical technique to measure the coating adhesion. The indenter imposes high stresses on the coating/substrate interface close to the edges of the impression. Poor adhesion can result in spalling or delamination of the coating. Thomas /18/ also used this indentation technique as a qualitative test on coated components. For alumina films deposited at low pressure and high temperatures, the load-displacement curves show numerous discontinuities, especially at low loads and low loading speeds. These unusual load-displacement curves were related to crack formation. At higher loads and loading speeds this effect was hardly observed, probably due to the lower sensitivity of the micro hardness tester. Optical microscopy showed that only small cracks at the edge and within the indentation were formed, the number being slightly smaller with increasing deposition temperature. The amount and the average length of the radial cracks were reduced with increasing deposition temperature. The fracture pattern of the alumina films generally shows circumferential cracks around the impression, which is more

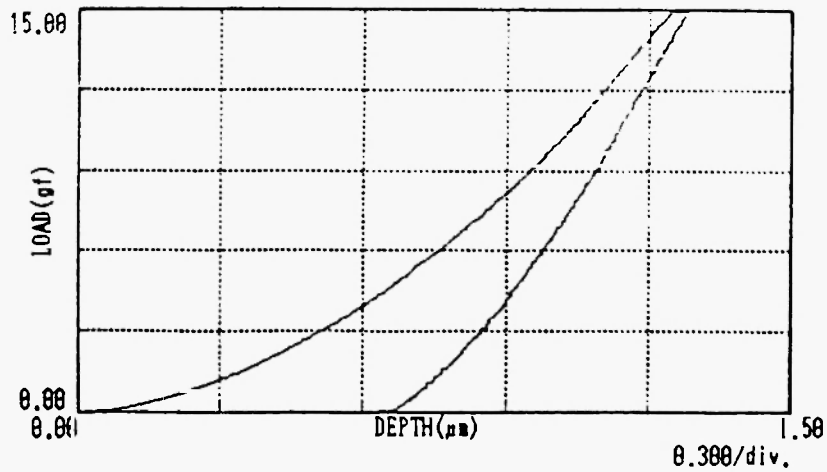

Fig. 12: A typical measured loading-unloading curve of amorphous alumina /4/.

pronounced with increasing film thickness. No significant changes were found in the cracking behaviour of alumina films deposited at different growth rates. The composite hardness increases with increasing deposition temperature. Figure 13 shows the surface morphology after indentation of the alumina films deposited at atmospheric pressure as a function of the film thickness. The length of the radial and lateral cracks can be used /6/ to evaluate the fracture toughness of the films and film/substrate interfaces. A semi-analytical relationship between the fracture toughness of the coating/substrate interface and the crack length is given by:

$$c^2 = \frac{\alpha_1 t^{\frac{3}{2}} H^{\frac{1}{2}} [1-(\frac{P_{cr}}{P})] P^{\frac{1}{2}}}{K_{Ic,\ interface}}$$

where c is the measured lateral crack length, P is the applied load, P_{cr} is the critical load, α_1 is a numerical constant, t is the film thickness, H is the mean hardness and K_{ic} is the fracture toughness of the film/substrate interface, respectively. From this equation it follows that the smaller the lateral crack length, the higher the fracture toughness of the film/substrate interface.

Again, in analogy with the fracture toughness of the film/substrate interface, the film fracture toughness can be calculated from the relationship

$$K_{Ic} = 0.129 \left(\frac{Ha^{0.5}}{\phi}\right)\left(\frac{E\phi}{H}\right)^{0.4}\left(\frac{L}{a}\right)^{-\frac{3}{2}}$$

where H is the film hardness, one half the indentation diagonal, ϕ a numerical constant, E the Young's modulus, and L the radial crack length.

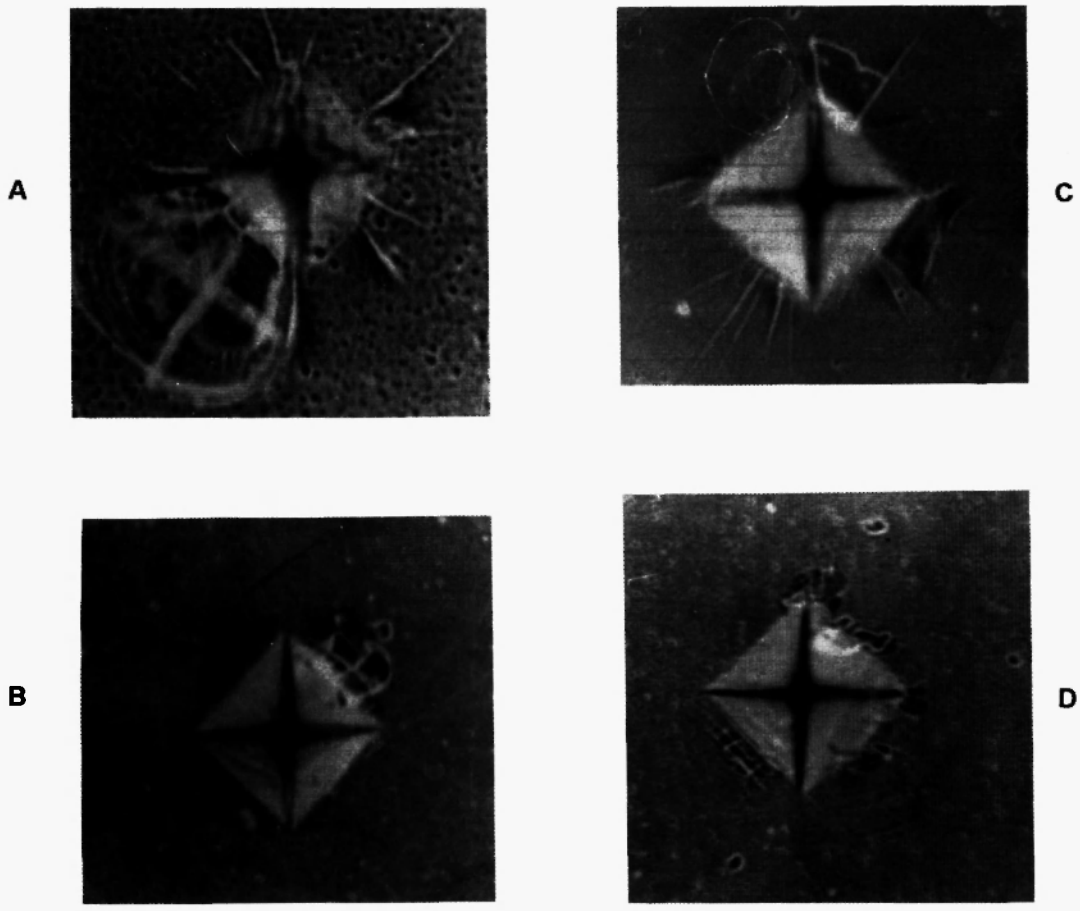

Fig. 13: Surface morphology after indentation of the alumina films deposited at atmospheric pressure as a function of the film thickness, a) 0.99 µm, b) 0.69 µm, c) 0.49 µm, and d) 0.25 µm /6/.

In order to obtain the critical load corresponding with the initiation of the crack formation, it is recommended that the micro-indentation system be extended with acoustic emission measurements, implying that the load-displacement can be followed continuously relating to fracture and plastic deformation of the materials. Crack growth, delamination and dislocation glides are related to sudden changes in stress. This change in energy will be sufficiently large and rapid so that ultrasonic vibrations are generated and can be monitored.

More information about the adhesion properties of the oxide film/substrate combination was obtained using the scanning scratch adhesion test. For alumina films, it was found that the critical load, for coatings deposited at low as well as at atmospheric pressure, increased with increasing coating thickness. In this case no difference was observed between the critical loads of the coatings deposited at reduced and at atmospheric pressure. With increasing partial pressure of the ATSB (increasing growth rates) the critical load of AP-MOCVD reduced from 130 to almost 70 mN. The critical load of the LP-MOCVD alumina films did not significantly change with varying partial pressures of the ATSB. No effect could be found of the critical load as a function of the deposition temperature. The average critical load for the alumina films (0.5 μm) deposited at atmospheric pressure is about 85 mN, and for the films deposited at reduced pressure about 80 mN. Scanning scratch test measurements were also performed by Hofman /4/. In addition to a review of several failure modes during scratch adhesion testing and a theoretical approach considering the estimation of the adhesion of films to a substrate, results were presented on the adhesion properties of silica films on Incoloy 800H and AISI 304. The critical load for the silica coatings on AISI 304, as determined by the scanning scratch tests, increases with increasing film thickness and increasing water concentration. The critical load for the silica film on Incoloy 800H also increases with increasing film thickness, but decreases with increasing water vapour. The adhesion from the scratch test results for the silica coatings on Incoloy 800H was always better than on AISI 304. Figure 14 shows the critical load as a function of the coating thickness /4/.]

Scanning-scratch-tests were also conducted with titania coatings deposited between 290 and 410°C. It was found that there was an optimum in critical load at 310°C: 250 mN. This value is higher compared to those obtained from 0.5 μm alumina (80 mN), deposited on the same substrate AISI 304 and under the same scratch conditions.

For the silica and alumina films, it was found that with an increase in film thickness, the critical load also increases. This was explained by Steinmann *et al.* /19/ and Hummer *et al.* /20/ by the fact that the extent and mode of coating/substrate deformation caused by the

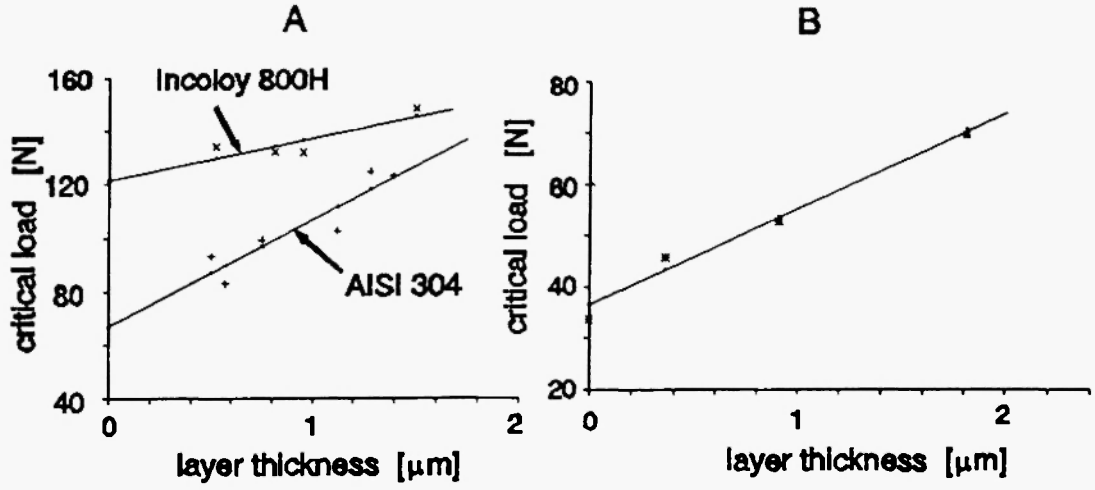

Fig. 14: The critical load as a function of the coating thickness, a) AISI 304 and Incoloy 800H, b) AISI 304 with 0.54 v% water vapour in the gas phase during deposition /4/.

stylus is mainly determined by the substrate deformation. The shear force is transmitted through the film by elastic and/or plastic deformation. Therefore, it is reasonable that an increased film thickness requires a higher load to obtain the same critical deformation for film cracking. Other aspects, for example, the use of different substrates or a post-deposition heat treatment, may affect the adhesion. Thermal annealing of thin alumina layers results in reduced adhesion strength. This was explained by sulphur segregation at the interface /21/. Hofman /4/ reported that the difference in adhesion strength between silica films deposited on Incoloy 800H and AISI 304 is partly attributed to the formation of an oxide scale on the alloy. In the case of Incoloy 800H, it is known that almost perfect chromia scales will form, while the scales on AISI 304 contain more defects and spinel phases. Therefore, it is reasonable to support that the interfaction between a closed chromia layer and the silica layer is better than between a spinel and a silica layer.

CONCLUSIONS

Metal-organic chemical vapour deposition of thin oxide films can be performed at relatively low temperatures and with simple production units.

The deposition of the desired oxide layer is related to the mechanism and the kinetic aspects of the decomposition. Depending on the molecular structure of the precursor, α-hydride elimination, β-hydride elimination, or a free radical mechanism dominates the overall mechanism. This also affects the kinetics, such as activation energy and reaction models (Langmuir adsorption model), of the film deposition.

The composition, and the chemical and mechanical properties of the thin oxide films are closely related to the process parameters, such as deposition temperature, reactor pressure and post-deposition thermal treatment (in air or in nitrogen at low pressure).

ACKNOWLEDGEMENTS

This research was supported by the Innovative Research Program on Technical Ceramics (IOP-TK) with the financial aid of the Dutch Ministry of Economic Affairs and the Technology Foundation (STW). Thanks are due to Mrs. M.M.D. Heusinkveld and Mr. J.G.F. Westheim for assisting in the experimental work.

REFERENCES

1. M.G. Hocking, V. Vasantrasree and P.S. Sidky, *Metallic & Ceramic Coatings,* Longman Scientific & Technical, John Wiley & Sons, Inc., New York, 1989.
2. E. Lang, *Coatings for High Temperature Applications,* Applied Science Publishers Ltd., London and New York, 1983.
3. M. Ohring, *The Materials Science of Thin Films,* Academic Press Ltd., London, 1992.
4. R. Hofman, "The Protection of Alloys Against High Temperature Corrosion by SiO_2-Coatings", PhD Thesis, University of Twente, The Netherlands, 1993.
5. R.W.J. Morssinkhof, "The Deposition of Thin Alumina Films on Steels by MOCVD", PhD Thesis, University of Twente, The Netherlands, 1991.
6. V.A.C. Haanappel, "Alumina Films on Metallic Substrates by MOCVD", PhD Thesis, University of Twente, The Netherlands, 1994.
7. V.A.C. Haanappel, H.D. van Corbach, T. Fransen and P.J. Gellings, *Thermochimica Acta,* **240,** 67-77 (1994).
8. S.B. Desu, *J. Am. Ceram. Soc.,* 72(9), 1615 (1989).
9. R. Hofman, J.G.F. Westheim, V.A.C. Haanappel, T. Fransen and P.J. Gellings, *Thermochimica Acta,* **215**, 329-335 (1993).
10. V.A.C. Haanappel, H.D. van Corbach, T. Fransen and P.J. Gellings, *High Temp. Mater. & Process.,* **12**(3), 127-138 (1993).
11. H.D. van Corbach, V.A.C. Haanappel, T. Fransen and P.J. Gellings, *Thin Solid Films,* **239**, 31-36 (1994).
12. R. Hofman, R.W.J. Morssinkhof, T. Fransen, J.G.F. Westheim and P.J. Gellings, *Mater. & Manuf. Process.,* **8**(3), 315-329 (1993).

13. H.D. van Corbach, private communications.
14. Yu.Yu. Baryshnikov, I.L. Zakharov and G.I. Makin, *Zhurnal Obshschei Khimii*, **60**, 1350 (1990).
15. C.J. Kang and J.S. Chun, *Thin Solid Films*, **189**, 173 (1990).
16. S.B. Desu, *Jap. J. Appl. Phys.*, **30**(12B), 2123 (1991).
17. B. Jonnson and S. Hogmar, *Thin Solid Films*, **114**, 257 (1984).
18. A. Thomas, *Surface Engineering*, **3**(2), 117 (1987).
19. P.A. Steinmann, Y. Tardy and H.E. Hintermann, *Thin Solid Films*, **154**, 333 (1987).
20. E. Hummer and A.J. Perry, *Thin Solid Films*, **101**, 243 (1983).
21. V.A.C. Haanappel, D. v.d. Vendel, H.D. van Corbach, T. Fransen and P.J. Gellings, *Oxidation of Metals*, **43**(5/6), 459 (1995).